Temporal Lobe Epilepsy: Anatomical and Effective Connectivity

Alex J. Cadotte, Thomas H. Mareci, Thomas B. DeMarse, Mansi B. Parekh, Rajasimhan Rajagovindan, William L. Ditto, Sachin S. Talathi, Dong-Uk Hwang, and Paul R. Carney, *Member, IEEE*

***Abstract*—While temporal lobe epilepsy (TLE) has been treatable with anti-seizure medications over the past century, there still remain a large percentage of patients whose seizures remain untreatable pharmacologically. To better understand and treat TLE, our laboratory uses several *in vivo* analytical techniques to estimate connectivity in epilepsy. This paper reviews two different connectivity-based approaches with an emphasis on application to the study of epilepsy. First, we present effective connectivity techniques, such as Granger causality, that has been used to assess the dynamic directional relationships among brain regions. These measures are used to better understand how seizure activity initiates, propagates, and terminates. Second, structural techniques, such as magnetic resonance imaging, can be used to assess changes in the underlying neural structures that result in seizure. This paper also includes *in vivo* epilepsy-centered examples of both effective and anatomical connectivity analysis. These analyses are performed on data collected *in vivo* from a spontaneously seizing animal model of TLE. Future work *in vivo* on epilepsy will no doubt benefit from a fusion of these different techniques. We conclude by discussing the interesting possibilities, implications, and challenges that a unified analysis would present.**

***Index Terms*—Connectivity, diffusion weighted imaging, Granger causality (GC), magnetic resonance imaging (MRI), temporal lobe epilepsy (TLE).**

Manuscript received February 11, 2008; revised July 18, 2008; accepted July 18, 2008. First published September 19, 2008; current version published July 06, 2009. This work was supported in part by the National Institutes of Biomedical Imaging and Bioengineering (NIBIB) through Collaborative Research in Computational Neuroscience (CRCNS) under Grant R01 EB004752 and Grant EB007082, in part by the Wilder Center of Excellence for Epilepsy Research, and in part the Children's Miracle Network. The work of P. R. Carney was supported by the Wilder Center of Excellence for Epilepsy Research Endowment funds. The work of W. L. Ditto was supported by the J. Crayton Pruitt Family Endowment funds. The work of S. Talathi was supported by a Fellowship Grant from the Epilepsy Foundation of America. The analysis work in this project was sponsored by the Office of Naval Research under Grant N00014-02-1-1019.

A. J. Cadotte and P. R. Carney are with the Department of Pediatrics Division of Pediatric Neurology, University of Florida, Gainesville, FL 32610 USA (e-mail: acadotte@peds.ufl.edu; carnepr@peds.ufl.edu).

T. H. Mareci is with the Departments of Biochemistry and Molecular Biology, University of Florida, Gainesville, FL 32610 USA.

T. B. DeMarse, R. Rajagovindan, and S. S. Talathi are with the Department of Biomedical Engineering, University of Florida, Gainesville, FL 32611 USA.

M. B. Parekh is with the Department of Neuroscience, University of Florida, Gainesville, FL 32608 USA.

W. L. Ditto was with the Department of Biomedical Engineering, University of Florida, Gainesville, FL 32611 USA. He is now with the Department of Bioengineering, Arizona State University, Tempe, AZ 85287 USA.

D.-U. Hwang was with the Department of Biomedical Engineering, University of Florida, Gainesville, FL 32611 USA. He is now with the Korea Institute of Oriental Medicine, Daejon 305-811, Korea..

Color versions of one or more of the figures in this paper are available online at http://ieeexplore.ieee.org.

Digital Object Identifier 10.1109/TNSRE.2008.2006220

I. Introduction: The Hippocampal Formation, A Test Bed for Neural Dysfunction and Epilepsy

EPILEPSY is the propensity to have seizures and is one of the most common serious neurological conditions, affecting 0.4%–1.0% of the world population [1]. Temporal lobe epilepsy represents approximately 60% of all partial epilepsies [2]. It is a well-established clinical observation that epileptic patients exhibit a high frequency of temporal lobe foci, often coupled with the neuropathological finding of mesial temporal lobe hippocampal sclerosis. As a result, the hippocampus has been a focus of interest in epilepsy research. Anatomically, the hippocampus is functionally organized in a parallel feed-forward fashion and contains several distinct layers [3]. The hippocampus also contains several well-described neuronal circuits such as the trisynaptic intrahippocampal pathway, which is linked to seizure onset. This provides an interesting structure for fundamental investigations into networks changes associated with epileptogenesis and ictogenesis in temporal lobe epilepsy. The trisynaptic pathway contains several coherent neuronal pathways such as Schaffer collaterals, perforant and mossy fiber, that are significantly altered in temporal lobe epilepsy.

The experimental and computational studies we present herein are consistent with the view that the hippocampus circuitry is composed of functionally specialized local population of neurons that are interacting dynamically during seizure along reentrant anatomical loops and pathways, within and between hippocampi. These large-scale patterns of temporal activity generated by the dynamics of neuronal interactions across the brain are often referred to as functional or effective connectivity. Clearly, a system's dynamics must strongly depend upon the underlying structure of the network. In the case of the brain, this structure is equivalent to its neuroanatomy. Functional integration accompanying seizures and limbic network changes are associated with patterns of functional and effective connectivity expressed across distributed neuronal groups and areas. Hence, there is an increasing amount of empirical evidence for the importance of functional connectivity in limbic epilepsy.

In recent years, neurophysiological and neuroimaging experiments, as well as detailed computer simulations, have contributed to our understanding of the neural mechanism generating functional connectivity [4]. Recently noninvasive imaging of the living brain has created tremendous enthusiasm for developing suitable methods. Of these methods, magnetic resonance imaging (MRI) can provide a great deal of information about anatomic structure (traditional imaging sequences), structural connectivity (diffusion weighted imaging), and function (functional MRI and MR spectroscopy) information at the same time on a single animal or human during the progression of a disease. Thus MRI can be used to create longitudinal

models in the four dimensions of time and space. In addition, the possibility of integrating MRI with other measures of brain function, like magnetoencephalography and high-resolution scalp and cortical electroencephalography, will open a unique "window" on the brain. Studies that have employed these techniques in isolation have produced important findings about nature of brain structure and function yielding important insights into how neural circuits work and how they break down in brain disorders. It is postulated that, anatomical and effective connectivity tools used in parallel may result in more advanced insights into the complex changes that occur during epilepsy.

In this paper, we review novel measurements of effective and anatomical connectivity. We then demonstrate, with experimental results, the effective patterns of local circuits in the hippocampus and pathways linking distinct subfields with the hippocampus in an experimental rat model of spontaneous limbic seizures. Subsequently, we present novel anatomical tools, measures, and results, which reveal structural brain connectivity through brain imaging. Finally, we discuss the advantages and challenges of relating effective and structural connectivity.

II. Effective Connectivity Methods in Epilepsy

One of the challenges facing neurologists in the study of epilepsy is of understanding how structural changes in the brain can lead to modifications in the behavioral output, i.e., activity, between different brain regions. Two broad categories of algorithms, functional and effective connectivity, have been used to extract these relationships from time series collected from various brain regions [6]. The delineation between these two types of connectivity is often unclear in the neuroscience community [7]. However, we draw from the definitions summarized by Sporns in a recent article on brain connectivity [8] to help differentiate between these two classifications [6]. Quoting directly from Sporns' article, "functional connectivity captures patterns of statistical dependence, while effective connectivity attempts to extract networks of causal influences of one neural element over another." Correlation and coherence are commonly used examples of functional connectivity, while partial directed coherence and Granger causality (GC) are examples of effective connectivity measures. In the following section, we will review specifically effective connectivity measures with an emphasis on their use in the study of epilepsy. We will also provide novel results from our application of an effective connectivity analysis tool, GC, which provides a strong and intuitive mathematical basis to determine causal influence and direction of neural interactions.

A. Effective Connectivity in Epilepsy

GC is an increasingly popular tool to understand the dynamic interactions of brain circuitry. New formulations have evolved within the GC toolset to better address the complexity of the neural systems being analyzed including pairwise, spectral, conditional [5], and multivariate block [6] GC. Pairwise Granger causality (PGC), considered to be the original GC formulation, is used to investigate directional interactions specifically between two time series. (We will use PGC to refer to this specific formulation and GC to describe the general family of Granger formulations from this point forward). The basic idea behind GC can be traced back to Wiener [7]. He proposed that, for two simultaneously measured time series, one series can be called causal to the other one if we can better predict the second series by incorporating past knowledge of the first one. This concept was later formalized by Granger in 1969 [8] for linear regression models of stochastic processes. Specifically, if the variance of the prediction error for the second time series at the present time is reduced by including past measurements from the first time series in a linear regression model, then the first time series can be said to have a causal (directional or driving) influence on the second time series.

Autoregressive (AR) models [9] are the core of parametric GC methods. A general form for the AR model is shown in (1), where $\boldsymbol{X}$ is a vector consisting of stationary time series from p channels, $\boldsymbol{A}$ is a $p\times p$ coefficient matrix and $\boldsymbol{E}$ is the uncorrelated noise vector with a covariance matrix of Σ

$$\boldsymbol{X}(t)+\sum_{m=1}^{p}\boldsymbol{A}(m)\boldsymbol{X}(t-m)=\boldsymbol{E}(t). \tag{1}$$

A univariate AR model predicts the current value of the variable from the past instances of the same variable. A multivariate AR (MVAR) model uses the same framework to model the current value of a variable using not only past instances of the same variable, but also past instances of the other variables in that multivariate system. The coefficient matrix $\boldsymbol{A}$ and the noise covariance Σ may be estimated by solving the Yule–Walker equations [10]. Model order $\boldsymbol{p}$ to achieve a optimal model fit for the data is typically estimated by minimizing the Akaike's information criterion (AIC) [11].

GC methods make use of the variance of prediction errors [predictions errors are $\varepsilon(t),\beta(t),\eta(t)$, and $\gamma(t)$ from (2) and (3)] to determine causal relationships. Consider two time series $\mathrm{X}(t)$ and $\mathrm{Y}(t)$ where an AR model is fit to each time series to predict current value of that time series say, X from p (p is a previously determined AR model order) past values of X

$$\begin{aligned} X(t)&=\sum_{j=1}^{p}b_{XX}(j)X(t-j)+\varepsilon(t)\\ \Sigma_1&=\mathrm{var}(\varepsilon(t))\\ Y(t)&=\sum_{j=1}^{p}b_{YY}(j)Y(t-j)+\gamma(t)\\ \Gamma_1&=\mathrm{var}(\beta(t)). \end{aligned} \tag{2}$$

The variance of the error series $\varepsilon(t),\Sigma_1$, is a gauge of the linear prediction accuracy of $X(t)$ as Γ_1 is for $Y(t)$. Now consider a second AR model, a bi-variate autoregressive model, $\boldsymbol{W}(t)$, where the current value of each time series say $X(t)$ and $Y(t)$ is predicted incorporating the p (from $j=1$ to p, same model order as the first AR model) past values of both the X and Y time series, shown in (3). Here, a_{XX},a_{YY},a_{XY}, and a_{YX} are the AR model coefficients

$$W(t)=\begin{pmatrix} X(t)=\sum_{j=1}^{m}a_{XX}(j)X(t-j)+\sum_{j=1}^{m}a_{\mathrm{XY}}(j)Y(t-j)+\eta(t)\\ Y(t)=\sum_{j=1}^{m}a_{YX}(j)X(t-j)+\sum_{j=1}^{m}a_{YY}(j)Y(t-j)+\gamma(t) \end{pmatrix}. \tag{3}$$

The variance of the new error series is a gauge of the prediction accuracy of the new expanded predictor

$$\Sigma_W = \begin{pmatrix} \Sigma_2 & \Upsilon_2 \\ \Upsilon_2 & \Gamma_2 \end{pmatrix} = \begin{pmatrix} \mathrm{var}(\eta(t)) & \mathrm{cov}(\eta(t),\gamma(t)) \\ \mathrm{cov}(\eta(t),\gamma(t)) & \mathrm{var}(\gamma(t)) \end{pmatrix}. \quad (4)$$

Based on Wiener's idea, Granger [8] formulated that if the X prediction is improved by incorporating past knowledge of the Y series, the Y time series can then be said to have a Granger-causal influence on the X time series. This is the basis for the time domain version of PGC where the variance of the linear prediction error of X alone, Σ_1, is compared to the variance of linear prediction error of X incorporating Y, Σ_2, shown in

$$F_{Y\to X} = \ln \frac{\Sigma_1}{\Sigma_2}. \quad (5)$$

Essentially, $F_{Y\to X}$ is the ratio of prediction error variance when only X's past values are incorporated to the prediction error variance when both $X$and Y's past information are incorporated. Note that when $\Sigma_1 = \Sigma_2$ (i.e., the linear prediction error is not improved by including Y) that this relationship will yield a PGC value of zero. Thus, when Y improved the prediction of X a causal relationship can be shown to exist. Causal influences in the opposite direction (X to Y) are addressed by simply reversing the roles of the two time series. It is clear from this definition that timing plays an essential role in directional causal influences. For a more detailed exposition of AR modeling and GC, please refer to a recent article [12] that discusses several of the GC formulations.

GC is now increasingly being applied in various neuroscience paradigms including *in vivo* plasticity [13], [14], functional connectivity using fMRI [15], [16], human sleep analysis [17], and connectivity within complex neural systems [18], [19]. Over the years, the framework of GC has been extended to more than two channels hence providing a true multivariate measure of causality. More sophisticated effective connectivity analysis in the frequency domain have also been introduced including approaches employing Geweke's frequency domain representation of time domain GC [5], [12], [20]–[22], partial directed coherence (PDC) [23], and directed transfer function (DTF) [22], [24] all of which fall under the framework proposed by Granger [8]. Mathematically, a theorem proven by Geweke [20], [21] promises deeper insights. It states that the total interdependence between A and B can be decomposed into three contributing factors: $(A \to B), (B \to \mathrm{A})$ and $(A.B)$. The arrow indicates causality in the Granger sense and $(A.B)$ signifies instantaneous causality or instantaneous correlation in the time series. The ability of Geweke's framework to also decompose the spectral density of the time series into an intrinsic part and a causal part enabled to quantify linear causality in the frequency domain for the first time. Given the predominance of oscillatory activity in the brain, such a tool offers immense ability to identify causal influences over functionally relevant frequency bands. Simple pairwise GC measures discussed in the previous section face a problem when considering more than two time series, since it cannot differentiate between direct and mediated (indirect) causal influence. Consider a simple network with three nodes X, Y, and Z with X driving Y and Y in turn driving Z. A simple PGC analysis on this network will yield the result $X \to Y, Y \to Z$ and a spurious causal influence $X \to Z$. In this case PGC cannot differentiate between a lack of direct causal influence between X and Z and a mediated or indirect influence of X on Z through Y. Geweke [21] proposed a version of conditional GC in order to overcome the detection of spurious causal patterns due to mediated influences from other time series. More recently, alternative measures for identifying causal interactions in neurobiological time series for multiple channels in the frequency domain under the same framework of GC are finding prevalence, which includes DTF, PDC, and direct DTF.

Referring to multivariate autoregressive model in (1), transforming this equation to the frequency domain yields

$$A(f)X(f) = E(f) \quad (6)$$

where

$$A(f) = -\sum_{j=0}^{p} A(j)e^{-i2\pi fj}. \quad (7)$$

Rewriting (6)

$$X(f) = H(f)E(f) \quad (8)$$

$H(f)$ is the transfer matrix of the system, where $H(f) = A^{-1}(f)$. In the case of DTF, the measure of causal influence from channel j to channel i is quantified in a normalized form as

$$\delta_{j\to i}(f) = \frac{|H_{ij}(f)|^2}{\Sigma_l |H_{il}(f)|^2} \quad (9)$$

which is the ratio of causal influence of channel j on i to the net influence from all other channels on channel i. This quantity has a desirable property of taking a value between 0, the case of no causal influence, and 1, a case of strong causal influence. DTF being a multivariate approach has the advantage of requiring only a single model fitting over all channels to be analyzed in contrast to PGC which requires model fitting over every pair of channels, however DTF has the same disadvantage of PGC, in that distinction can not be made as to whether the observed causal influence is direct or mediated, hence leading to detection of spurious direct influence when only an indirect influence exists. A recent study has suggested that this ambiguity may be mitigated by a simple operation of multiplying a variant of the DTF measure (following a slightly different normalization procedure where the denominator of (9) is summed across all frequencies) by the corresponding partial coherence of the channel pair and have named this approach the direct DTF (dDTF) [25].

Another widely used measure for simultaneous connectivity analysis of more than two channels in the frequency domain is the PDC [26]. The PDC is based on the previously described concept of partial coherence and may be thought of as a factorization of the symmetric partial coherence measure into factors quantifying the direct causal influence between the two time series (10), [23]

$$\kappa_{ij}(f) = \pi_i^H(f)\Sigma^{-1}\pi_j(f) \quad (10)$$

where $\kappa_{ij}(f)$ is the partial coherence between channels i and j and $\pi_{ij}(f)$ is the partial directed coherence factor. In order to

remove the contribution of instantaneously correlation between the channels from the direct causal influences, the factor terms in (10) is simplified to

$$\bar{\pi}_{j\to i}(f) = \frac{|A_{ij}(f)|}{\sqrt{\Sigma_k |A_{kj}(f)|^2}} \tag{11}$$

where $A_{ij}(f)$ is the element in the ith row and jth column of $A(f)$ in (7) and $\pi_{j\to i}(f)$ is defined as the PDC measure of causal influence of channel j on channel i. It may be noticed that the normalization factor in (11) is the net outflow of information or coupling strength of the driving channel to all other channels.

If the number of channels analyzed is two, then PDC and DTF are equivalent to the PGC measure. Since PDC is based on partial coherence it is inherently insensitive to mediated or indirect causal influences from other channels in comparison to DTF or PGC. Direct causality measures such as PDC, dDTF, and conditional GC have been successfully used in several recent studies and the results in terms of the direction of influence have often been found to be in agreement with each other [12], [23], [27]–[31]. For a comparison of the strengths, weaknesses, and the performance of these three methods in various circumstances please refer to [28].

Several of these causality measures have proven to be useful tools in the study of epilepsy. The first applications of the DTF to seizure can be traced back to Franaszczuk *et al.* [32]–[34] where seizure time series from subdural grids and depth electrodes in humans were analyzed to determine seizure onset and propagation patterns. Two recent articles [35], [36] demonstrate the utility of the PDC for finding the focus of seizure onset in human patients observed using the standard $10/20$ EEG system. Such localizing ability may provide crucial information in the selection of cortical/subcortical areas for resection, effectively treating or ameliorating the occurrence of seizures in a patient. Additionally in these studies, the causal flow during seizure was observed before, during, and after seizure using 24 EEG channels sampled at 200 Hz in a single patient. It was observed that during seizure the causal influence radiates away from areas that may most likely represent the focus of seizure onset in the left temporal lobe of the patient. PDC and the DTF have also produced meaningful results in the analysis of neural time series including EEG [37]–[39], neural simulation [39], [40], and living neural networks *in vivo* [41]–[43].

In the following section, we present preliminary results on the use of PGC to explore the dynamic interactions between different hippocampal areas during seizures recorded from *in vivo* microwire arrays implanted into the hippocampus of spontaneously seizing rats.

B. Results: Spontaneous Temporal Lobe Seizure Analysis Using GC

Animal Model: All experimental protocols and procedures involving animals and their care were conducted in conformity with NIH and IACUC committee at the University of Florida. The animal model employed has been studied for the last two decades [44], [45]. The main characteristic of this model is that an initial seizure, induced by electrical stimulation from an electrode placed in the hippocampus, eventually leads to spontaneous seizures in 4–6 weeks. This model closely resembles the symptoms of human patients that have chronic mesial temporal seizures [46]–[48]. 16-electrode microelectrode arrays were implanted in each brain hemisphere with the electrode tips located within the CA1 and DG regions of the hippocampus. Our experiment consisted of 63-day-old adult male Sprague Dawley rats $(n = 5)$, weighing between 200–265 g, with 16 50-mm-diameter microwire recording electrodes implanted bilaterally into the CA1, CA3, and dentate gyrus regions of the hippocampus. In addition, a bipolar pair of Teflon-coated, tungsten electrodes, 50μm in diameter, was implanted for acute electrical stimulation into the right posterior ventral hippocampus. After one week of baseline EEG recordings at a sampling rate of 12 kHz, rats were electrically stimulated for 30 min until sustained behavioral and electrographic seizures were observed. Rats stopped seizing after approximately eight hours, after which they entered a seizure-free latent period. Rats were then monitored with continuous video-EEG and screened for the occurrence of their first spontaneous seizure at two to four weeks post status epilepticus. At the end of the recording session, the rats were sacrificed and the intact brains were excised. The isolated intact brains were imaged with a high-field resonance microscopy to confirm the location of the electrode placement within the hippocampus, as is shown in Fig. 2.

The continuous EEG recordings were screened for seizures using an offline automated seizure detection algorithm [49] and verified by an expert epileptologist used this electrographic and video evidence to detect seizure events. A 1-min window preseizure and a similar window including the seizure was extracted from the raw recording and low pass filtered to 1 kHz. PGC was then calculated between all combinations of the 32 channels for each of these windows to understand how gross effective connectivity differs between these two brain states. The AR model order was optimized at $m = 25$ using the AIC described earlier. The Yule–Walker equations were solved using Morf's method [50]. An analysis where PGC was calculated from four seizures (60 s pre- and during each seizure was used a realization in the PGC analysis) as well as from interictal epochs from the same subject is shown in Fig. 1. The causal interactions between all electrodes immediately preseizure are shown in panel A. During seizure interactions are shown in panel B. Analysis of interictal epochs far removed from seizure are shown in panel C. The statistical significance of these interactions was addressed by creating a time shuffled surrogate of the preseizure and seizure data that was also analyzed using PGC, shown in panel D. Note that the patterns shown in panels A and B are obliterated in panel D as the time shifted surrogate has no coherent causal structure. This surrogate analysis yielded a significance threshold of 2.29 $(P < 0.01)$. Thus, all values below 2.29 in both panel A and panel B are considered to be indistinguishable from noise and are not displayed. A surrogate analysis was also carried out for the interictal epoch shown in panel C yielding a significance threshold of 1.52 $(P < 0.01)$. Please note that panel C uses the same color scale as the other panels so that the colors represent equivalent magnitudes in all panels. This analysis is similar to previous causal analysis of *in vivo* seizure [35], [36]. However, higher spatial resolution is achieved from the use of microelectrodes that are implanted into the regions of interest rather EEG electrodes

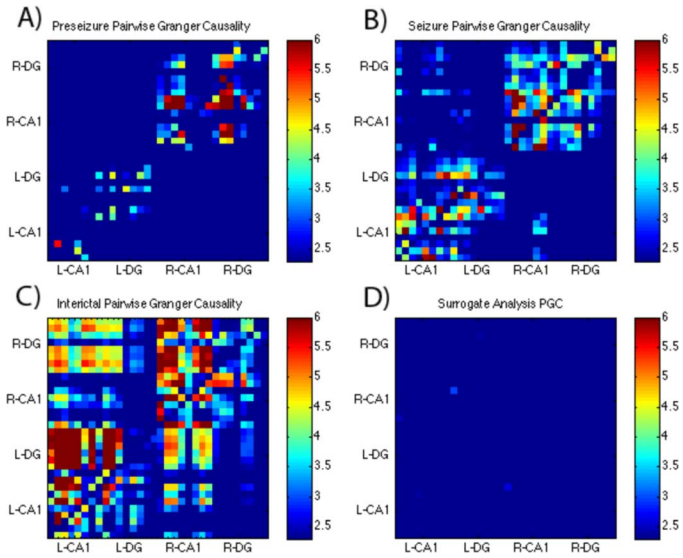

Fig. 1. Pairwise GC interactions between all electrodes for immediately preseizure (A), during seizure (B), interictal (C), and surrogate (D) analyses. Each pixel in these plots is described by three attributes; source electrode (*y*-axis), destination electrode (*x*-axis), and magnitude of PGC interaction by color (PGC magnitude shown in the color bars for each panel, dark blue is considered to mean no significant interaction). Comparison of A and B indicates that there is a significantly larger amount of directional synchronization during seizure (panel B) than preseizure (panel A) ($p < 0.01$). Panel C shows the interictal causal relationships when the animal is awake and freely exploring its environment. Panel D shows the surrogate analysis, created by time shifting the time series used to create panels A and B. Notice that the patterns shown in panel B have been obliterated. Surrogate analysis suggests a threshold value of 2.29 ($p < 0.01$) above which the interactions is significantly different than random. The color scale begins at 2.29 in all plots (see online version to resolve colors) to remove nonsignificant interactions from these plots.

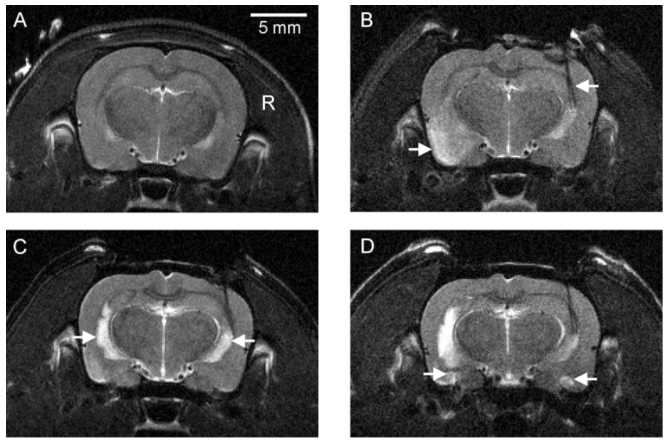

Fig. 2. MR images (coronal T2-weighted) at 11.1 T from the same slice location during the epileptogenic period. Part A is preimplant, preinjury (5 mm length-scale bar, R on brain right side). Part B is three-day postsimulation, where right-side arrow indicated the simulating electrodes and left-side arrow regions of hyper-intensity in E/PC. Part C is at day 20, with regions of hyper-intensity seen in the on both sides (arrows) in the region of the hippocampus and lateral ventricles. Part D is at day 60 illustrate the increase in the hyper-intensity within the E/PC and additional regions of hyper-intensity in the amygdala on both sides of the brain (arrows).

placed on the brain surface. Each pixel in these plots is described by three attributes; source electrode (*y*-axis location), response electrode (*x*-axis location), and magnitude of PGC interaction (represented by the color scale displayed with the panels where dark blue represents no significant interaction and red representing the strongest interactions).

Comparison of panels A and B suggests that there is a significantly larger amount of directional synchronization during seizure (left panel) than preseizure (right panel) ($F(1,2) = 245.67, p < 0.001$ for all 1024 interactions, pre versus during). Synchronization of neural units across a diffuse excitable network is thought to be a possible mechanism that initiates seizure in the limbic system. [51]. Also note that in the preseizure panel there are no significant directional influences between hemispheres (top left and bottom right quadrants of panel A). The during-seizure panel on the right clearly shows there are between hemisphere interactions during seizure ($F(1,2) = 474.55, p < 0.001$ for the 512 between hemisphere interactions, within top left and bottom right quadrants, panel A versus panel B, for all PGC values above and below surrogate threshold). Also of interest is the substantial preseizure synchronization from the R-CA1 to the R-DG shown as bright red areas in the top right of panel A. These preseizure interactions are not only anatomically unexpected, but may indicate the beginnings of the synchronization process that leads to full seizure. If this were true, this may indicate that the seizure spread outward from the R-CA1. A general visual comparison of panel C to panels A and B suggests that the interactions during normal awake exploratory behavior, panel C, are radically different from panels A and B. One reason may be that the animal is usually still asleep during the preseizure recordings, panel A. However, the causal interactions between and within hemispheres during these interictal epochs appear to be more balanced between hemispheres, as in panel C, rather than dominated by higher synchronization in the right hemisphere, as in panel A. Additionally, the dominant interictal influences are directed from the CA1 regions to the DG regions within both hemispheres ($F(1,2) = 44.45, p < 0.01$, when comparing CA1 to DG versus DG to CA1 over both hemispheres). This result agrees with the expected structural and anatomical pathways within the trisynaptic pathway of the hippocampus [52].

The use of effective connectivity measures has lead to a new understanding of the interactions within the hippocampus during seizure. In future work, functional and effective connectivity from causal analysis could be used in parallel with structural imaging protocols such as MRI. This would provide a strong linkage between observed functional changes and anatomical changes during the latent phase of epileptogenesis. In the following section, we discuss magnetic resonance based structural connectivity methods used by our multidisciplinary team in the study of temporal lobe epilepsy.

III. Visualization of Structural Connectivity Using MR

Physiological measurements of brain function can be put into the context of the evolving injury, during the epileptogenic period, by visualizing brain structure with MRI. To accomplish this, we have developed an MRI protocol to examine the rat brain *in vivo*. At 11.1 T (470 MHz) we measure preinjury control images, postelectrode-implant images, then images at 3, 5, 7, 10, 20, 40, and 60 days following injury. The animal is sacrificed

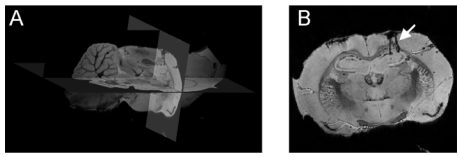

Fig. 3. MR image of excised brain at 17.6 T. Part A is a view of three orthogonal slices through the 3-D MR image. Part B is the coronal slice, from the image in part A, showing the placement of two representative recording electrodes (indicated by the arrow).

after day 60, the brain is fixed, then excised for further study. MR images of the intact, fixed, excised brain are acquired in very high-resolution MR images at 17.6 T (750 MHz). Finally, the brain is destructively processed for histological analysis. For both the MR images acquired *in vivo* and with the excised intact brain, we measure anatomical images, quantify MR relaxation times, and measure diffusion weighted images.

A. In Vivo Magnetic Resonance Imaging

MR images of each rat were measured *in vivo* at 11.1 T (shown in Fig. 2) with a multiple-slice, multiple-spin-echo sequence with segmented phase encoding and a field of view 30 mm $\times$ 30 mm in 0.9 mm slices. These images were measured from the same slice locations during the period of epileptogenesis. In part A, the coronal T2-weighted image shows the normal appearing contrast in the rat brain prior to electrode placement and simulation. White matter (e.g., corpus collosum) has a shorter transverse (T2) relaxation time than the gray matter, so white matter appears darker, than the surrounding gray matter, in these T2-weighted images. The image in part B was taken three days after stimulation and shows the location of the Teflon-coated bipolar simulation electrodes and regions of hyper-intensity in entorhinal/piriform cortex (E/PC), contra-lateral to the location of stimulation. The hyper-intensity appears to results from edema, which resolves after a few days (see Part C). Part C illustrates the continued evolution of the injury at day 20. Regions of hyper-intensity are seen on both sides of the brain in the region of the hippocampus and lateral ventricles and appear to represent the early stages of tissue loss and cavity formation. Part D shows the final image at day 60 following injury and illustrate the increase in the hyper-intensity (probably cavity formation) within the E/PC and additional regions of hyper-intensity (also probably cavities) in the amygdala on both sides of the brain.

After the final image in collected *in vivo* at day 60, the fixed intact brain is extracted and imaged with very high-resolution images at 17.6 T. Representative image data is shown in Fig. 3. A gradient echo 3-D image has measured with a resolution of 75 μm $\times$ 75 μm $\times$ 75 μm. In Part A, the complete image data is visualized with three orthogonal slices and in part B, the tracts of two recording electrodes are shown in the coronal slice from part A. While the MR images of the rat brain *in vivo* and as excised tissue provide important information, the most informative structural information is provided by the diffusion weighted images which can be modeled as either diffusion tensor images or as images of water displacement probability maps.

B. Diffusion Weighted Imaging

Animal studies have shown that diffusion-weighted MRI (DWI) can visualize the histo-pathological changes that result from seizures [53]. However it has become apparent that knowledge of the white matter connections is crucial to the understanding of normal and abnormal brain function [54]. With conventional MRI, variations in white matter signal are subtle, and white matter tracts cannot be accurately parcellated. But tissue structures restrict the diffusion of water [55], [56] and this can be visualized with DWI. The effect of water diffusion on MR images is modeled in two ways: 1) diffusion tensor imaging (DTI), using a rank-2 tensor representation, and 2) the calculation of a water displacement probability in each voxel. In the DTI model, the direction and rate of water diffusion are represented by a positive-definite rank-2 tensor [57]. This approach allows a simple estimation of diffusion anisotropy, through the calculation of orientation-independent fractional anisotropy, and can be used to infer fiber orientation [58], [59]. Despite the model simplicity, DTI can successfully visualize regions of the central nervous system with substantial white matter coherence and has allowed the mapping of many anatomical connections [60]–[62].

In both animal models of TLE and in human patients with TLE, DWI, and DTI have been used to describe structural changes at different stages of epilepsy. In animal studies, the rate of water diffusion has been observed to decrease within the seizure foci during induced SE [63], probably due to the redistribution of water from the extracellular to the intracellular space resulting from an alteration of cell membrane permeability brought about by long-term excitation of the cells [64], [65]. This swelling of the neuronal cell bodies and processes leads to an increase in the tortuousity of the water diffusion path in the cortex and therefore results in a subsequent decrease in measured diffusion rate. A decrease in the rate of diffusion during and within a few hours after the onset of SE (in the amygdala, and the piriform cortex) has been associated with ongoing neuronal cell death that was observed 24 h post-SE [64] and two weeks post-SE [66].

A chronic elevation of diffusion rate is observed in TLE patients with hippocampal sclerosis, which has been attributed to neuronal necrosis, gliosis, and expanded extracellular space [67]. Using DTI, increased diffusion rate and a decreased diffusion anisotropy in the epileptic focus, compared to the contralateral region, was observed by Assaf *et al.* [68] in patients with TLE. Similar studies using DTI have reported a reduction in diffusion anisotropy in the ipsilateral parahippocampal gyrus and fornix [69], and also in extra-temporal white matter, such as the internal capsule [70], the external capsule [71], the genu [70], and the splenium [71] of the corpus callosum. The reduction in diffusion anisotropy has been suggested to result from a loss of ordered structure, myelin degradation, and lowered cell density [69], [70], [72]. Fiber tract maps generated from DTI measurements have also shown a reduction in tract volume of the fornix both pre- [73] and post- [74] resective surgery of the epileptogenic focus, as well as an increase in diffusion rate and a decrease in diffusion anisotropy, in patients with unilateral TLE. The structural abnormalities in both gray and white

matter in patients with TLE occur over a large number of regions both within the temporal lobe and in regions associated with the temporal lobe. Yet very few animal studies have looked at both gray and white matter changes during the latent period of epileptogenesis.

However DTI fails to accurately represent complex tissue structure [58], [75], [76]. This limitation of the DTI approach can be overcome by the acquisition of high angular resolution diffusion images (HARDI) [77], [78], in which diffusion is measured at higher angular resolution along a large number of directions. Using this approach, the complexity of tissue structure can be visualized in each image voxel by determining the displacement probability for water in the tissue.

Several approaches to modeling the HARDI data have been proposed [75], [79]–[81]. As part of this effort, we have developed methods to visualize the diffusion displacement probability [79], [81]–[83] of fibrous structures in complex tissue regions in excised rat brains [83] and human brains *in vivo*. As part of this work, we developed a measure of displacement probability anisotropy, which provides a measure of tissue anisotropy [82] in complex tissue regions similar to that of the DTI-based factional anisotropy useful for simpler tissue regions. Using the direct estimation of the water displacement probability, we can visualize water-diffusion restriction in each voxel of an MR image to infer the tissue structure.

C. Results: Structural Connectivity Using HARDI

As an example, recent investigations in our laboratory, regarding the white matter structural changes following epileptogenesis, have revealed that MR HARDI methodology can identify changes in limbic system connectivity following the onset of epilepsy [81], [83]. The displacement probability maps for a control and injured excised rat brain, sacrificed $\sim$60 days following injury, are shown in Fig. 4. The relaxation-weighted images, in parts A and D, do not show much detail about the structural changes. More structural information is suggested in the fractional anisotropy images shown in parts B and E, but no specific information on connectivity is provide in these images. However, the displacement probability maps, shown in part D and F (expansion of the region, red boxes, around the hippocampus on the left side of the brain image), reveal the underlying structural changes in the hippocampus and surrounding structures. The displacement probability map in each voxel depicts the orientations of the highly anisotropic and coherent fibers. In the injured brain, the CA1-fimbria region appears much more disorganized relative to control.

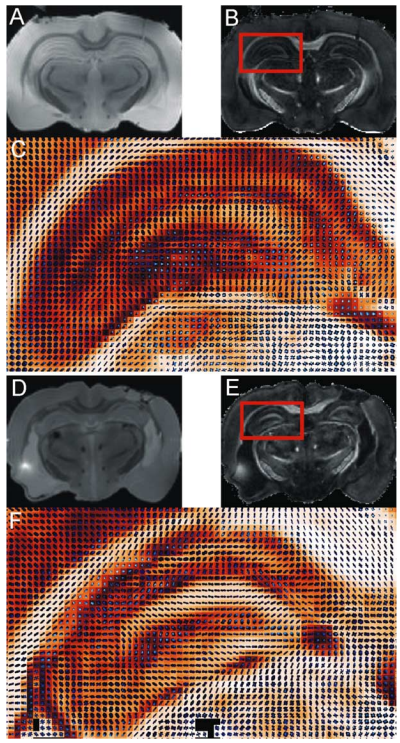

Fig. 4. MR diffusion weighted images and diffusion modeling are shown at 17.6 T. The relaxation-weighted images of a control rat brain are in part A and an injured brain in part D. The fractional anisotropy image derived from the rank-2 tensor model of diffusion is shown for a control brain in part B and an injured brain in part E. The displacement probability density maps are shown in part C for a control brain and an injured brain in part F. In part F, note both the loss of fiber structure in CA1, CA3, and hilar region, as well as changes in mossy fiber and Schaffer's collateral in the epileptic hippocampus. Diffuse reorientation of fibers is seen throughout and is most noticeable in the CA1 and mossy fiber regions.

IV. Conclusion

Combining information about anatomy and function is critical for the development of a complete understanding of nervous system processes [84]. Such structure-function information is fundamental to all processes in the CNS (normal and pathological), since anatomical connections determine where information is passed and how this information is processed in the brain. An approach to determining structure-function information has been demonstrated by Conturo *et al.* [60], who have used DWI to provide connectivity information related to the functional response of the brain during visual stimulation. They modeled the fiber connectivity of the brain with DTI then related that anatomical information to the measured functional response of the brain using functional MRI. Their work illustrates the power of the DWI methodology in determining structure information that can be related to measures of function, like electrophysiology. This approach is particularly important for the study of evolving pathology in the brain, such as epilepsy, where a method is needed that correlates structural connectivity with a measure of function.

The connectivity changes observed during epileptogenesis using DWI should logically be accompanied by changes in the electrophysiological behavior within our animal model of TLE. Indeed, abnormal seizure behavior and effective connectivity relationships are implied in our measurements over many subjects. However, the weakness common to both of these methods is that neither of them can independently elucidate the mechanisms for seizure generation. Indeed these methods will need to be combined to provide a complete description of the *in vivo* mechanisms behind seizure. It is not known whether the changes in anatomical connectivity occur before or after changes in effective connectivity. Thus, it is unclear whether abnormal function leads to structural changes or whether structural changes lead to abnormal function. Clearly, this paradox must be resolved in order to reveal the fundamental mechanisms of epileptogenesis.

Although significant changes in connectivity can be measured using the broad range of tools that we have reviewed in the paper, several questions remain unanswered. The most fundamental of these questions is how structural connectivity changes relate to function over the epileptogenic period. Future experiments would need to be carefully designed so that results from these analyses can be integrated and evaluated rigorously. But the underlying assumption, in the approach we have outlined here, is that the temporal relationship between functioning "units," as measured with GC, depends on a structural connectivity that can be measured with DWI. Thus, these methods should be able to elucidate the structure-function relationship in pathological situations, such as epilepsy. Therefore, both measurements will need to be performed in the same subject at the same time during the evolution of this pathology.

However, recording electrophysiological activity during MRI measurements is a formidable task made complex by the magnet environment [85]. In experimental animal models, recording electrodes (fabricated with materials currently in use) interfere with image acquisition. But the development of magnetic-susceptibility-matched recording electrodes, with an appropriate interface to the electrophysiological apparatus, may allow simultaneous EEG and MRI measurement in the magnetic fields of MRI systems. We are working on these fundamental problems in order to facilitate future experiments.

Ultimately, the critical test of this, or any approach, is the translation of these methods from the animal model to human TLE patients. Combining advanced methods, such as high-resolution micro-electrode arrays, effective connectivity analysis using GC, and DWI acquisition tools, for the study of the spontaneously seizing animal model of TLE will likely lead to a better understanding of the fundamental mechanisms underlying TLE and likely lead to new and innovated therapies for patients with TLE.

ACKNOWLEDGMENT

The authors would like to thank Dr. W. Norman and S. Myers for data collection and animal care and M. Guoan for reviewing the behavioral videos to identify the seizure events. The authors would like to thank Dr. M. Ding, Dr. A. Bollimunta, Dr. Y. Chen, Dr. B. Vemuri, and Y. Zhang for helpful discussions pertaining to analysis. The authors would also like to thank L. Hoang-Minh and H. Sepulveda for MR imaging assistance. MRI data were obtained at the Advanced Magnetic Resonance Imaging and Spectroscopy (AMRIS) Facility in the McKnight Brain Institute of the University of Florida.

REFERENCES

[1] J. Sander and S. Shorvon, "Epidemiology if the epilepsies," *J. Neurol. Neruosurg. Psychiatry*, vol. 61, pp. 433–443, 1996.

[2] R. Fisher *et al.*, "Epileptic seizures and epilepsy: Definitions proposted by the international league against epilepsy (ILAE) and the international bureau for epilepsy (IBE)," *Epilepsia.*, vol. 46, no. 4, pp. 470–472, 2005.

[3] R. Y. Cajal, "Estructura del asta de ammon," *Anales de la Sociedad Espanola de Historia Natural*, vol. 22, pp. 53–114, 1982.

[4] F. L. da Silva, , E. Niedermeyer and F. L. da Silva, Eds., "EEG analysis: Theory and Practice; Computer-assisted EEG diagnosis: Pattern recognition techniques," in *Electroencephalography: Basic Principles, Clinical Applications, and Related Fields*. Baltimore, MD: Wilkins & Wilkins, 1987, pp. 871–897.

[5] Y. Chen, S. L. Bressler, and M. Ding, "Frequency decomposition of conditional Granger causality and application to multivariate neural fielfd potential data," *J. Neurosci. Methods*, vol. 150, pp. 228–237, 2006.

[6] X. Wang *et al.*, "Granger causality between multiple interdependent neurobiological time series: Blockwise versus pairwise methods," *Int. J. Neural. Syst.*, vol. 17, no. 2, pp. 71–78, 2007.

[7] N. Wiener, , B. Ef, Ed., "The Theory of Prediction," in *Modern Mathmatics for Engineers*, ser. 1. New York: McGraw-Hill, 1956.

[8] C. W. J. Granger, "Investigating causal relations by econometric models and cross-spectral methods," *Econometrica.*, vol. 3, pp. 424–438, 1969.

[9] C. Chatfield, *The Analysis of Time Series an Introduction*, 5th ed. Boca Raton, FL: Chapman & Hall, 1996.

[10] M. Ding *et al.*, "Short-window spectral analysis of cortical event-related potentials by adaptive multivariate autoregressive modeling: Data preprocessing, model validation, and variability assessment," *Biol. Cybern.*, vol. 83, no. 1, pp. 35–45, Jul. 2000.

[11] H. Akaike, "A new look at the statistical model identification," *IEEE Trans. Autom. Control*, vol. 19, no. 6, pp. 716–723, Dec. 1974.

[12] M. Ding, Y. Chen, and S. L. Bressler, , Timmer, Schelter, and Winderhalder, Eds., "Granger Causality: Basic Theory and Application to Neuroscience," in *Handbook of Time Series Analysis*. New York: Wiley, 2007.

[13] L. Zhu *et al.*, "Probing changes in neural interaction during adaptation," *Neural Computat.*, vol. 15, no. 10, pp. 2359–2377, Oct. 2003.

[14] L. Q. Zhu *et al.*, "Characterization of neural interaction during learning and adaptation from spike-train data," *Math. Biosci. Eng.*, vol. 2, no. 1, pp. 1–23, Jan. 2005.

[15] R. Goebel *et al.*, "Investigating directed cortical interactions in time-resolved fMRI data using vector autoregressive modeling and Granger causality mapping," *Magn. Reson. Imag.*, vol. 21, pp. 1251–1261, 2003.

[16] J. R. Sato *et al.*, "A method to produce evolving functional connectivity maps during the course of an fMRI experiment using wavelet-based time-varying Granger causality," *Neuroimage*, vol. 31, no. 1, pp. 187–196, May 5, 2006.

[17] M. Kaminski *et al.*, "Evaluating causal relations in neural systems: Granger causality directed transfer function and statistical assessment of significance," *Biological Cybern.*, vol. 85, no. 2, pp. 145–157, Aug. 2001.

[18] A. K. Seth, "Causal connectivity of evolved neural networks during behavior," *Network-Computat. Neural Syst.*, vol. 16, no. 1, pp. 35–54, Mar. 2005.

[19] A. K. Seth and G. M. Edelman, "Distinguishing causal interactions in neural populations," *Neural. Comput.*, vol. 19, no. 4, pp. 910–933, Apr. 2007.

[20] J. Geweke, "Measurement of linear dependence and feedback between multiple time series," *J. Amer. Stat. Assoc.*, vol. 77, pp. 304–313, 1982.

[21] J. F. Geweke, "Measures of conditional linear dependence and feedback between time series," *J. Amer. Stat. Assoc.*, vol. 79, no. 388, pp. 907–915, 1984.

[22] M. Kaminski and K. Blinowska, "A new method of the description of the information flow in the brain structures," *Biol. Cybern.*, vol. 65, pp. 203–210, 1991.

[23] L. A. Baccala and K. Sameshima, "Partial directed coherence: A new concept in neural structure determination," *Biol. Cybern.*, vol. 84, no. 6, pp. 463–474, Jun. 2001.

[24] M. Kaminski *et al.*, "Evaluating causal relations in neural systems: Granger causality directed transfer function and statistical assessment of significance," *Biological Cybern.*, vol. 85, pp. 145–157, 2001.

[25] A. Korzeniewska *et al.*, "Determination of information flow direction among brain structures by a modified directed transfer function (dDTF) method," *J. Neurosci. Methods*, vol. 125, pp. 195–207, 2003.

[26] K. Sameshima and L. A. Baccala, "Using partial directed coherence to describe neuronal ensemble interactions," *J. Neurosci. Methods*, vol. 94, pp. 93–103, 1999.

[27] Y. H. Chen, S. L. Bressler, and M. Z. Ding, "Frequency decomposition of conditional Granger causality and application to multivariate neural field potential data," *J. Neurosci. Methods*, vol. 150, no. 2, pp. 228–237, Jan. 1, 2006.

[28] M. Winterhalder *et al.*, "Comparison of linear signal processing techniques to infer directed interactions in multivariate neural systems," *Signal Process.*, vol. 85, pp. 2137–2160, 2005.

[29] L. A. Baccala and K. Sameshima, "Overcoming the limtations of correlation analysis for many simultaneously processed neural structures," *Prog. Brain Res.*, vol. 130, pp. 33–47, 2001.

[30] R. Kus, M. Kaminski, and K. Blinowska, "Determination of EEG activity propagation," *IEEE Trans. Biomed. Eng.*, vol. 51, no. 9, pp. 1501–1510, Sep. 2004.
[31] L. Astolfi *et al.*, "Comparison of different cortical connectivity estimators for high-resolution EEG recordings," *Human Brain Mapp.*, vol. 28, no. 2, pp. 143–157, 2007.
[32] P. Franaszczuk and G. Bergey, "Application of the directed transfer function method to mesial and lateral onset temporal lobe seizures," *Brain Topogr.*, vol. 11, pp. 13–21, 1998.
[33] P. Franaszczuk *et al.*, "Time-frequency analysis using matching pursuit algorithm applied to seizures originating from the mesial temporal lobe," *Electroencephalogr. Clin. Neurophysiol.*, vol. 106, pp. 513–521, 1998.
[34] P. Franaszczuk, G. Bergey, and M. Kaminski, "Analysis of mesial temporal seizure onset and propogation using the directed transfer function method," *Electroencephalogr. Clin. Neurophysiol.*, vol. 91, pp. 413–427, 1994.
[35] L. A. Baccala *et al.*, "Graph theoretical characterization and tracking of the effective neural connectivity during episodes of mesial temporal epileptic seizure," *J. Integrative Neurosci.*, vol. 3, no. 4, pp. 379–395, 2004.
[36] D. Y. Takahashi, L. A. Baccala, and K. Sameshima, "Connectivity inference between neural structures via partial directed coherence," *J. Appl. Stat.*, vol. 34, no. 10, pp. 1259–1273, 2007.
[37] M. Kaminski, K. Blinowska, and W. Szelenberger, "Topographic analysis of coherence and propogation of EEG activity during sleep and wakefulness," *Electroencephalogr. Clin. Neurophysiol.*, vol. 102, pp. 216–227, 1997.
[38] J. Ginter *et al.*, "Propagation of brain electrical activity during real and imagined motor task by directed transfer function," in *Proc. 2nd Int. IEEE EMBS*, 2005, pp. 5–8.
[39] B. Schelter *et al.*, "Testing for directed influences among neural signals using partial directed coherence," *J. Neurosci. Methods*, vol. 152, no. 1–2, pp. 210–219, Apr. 4, 2006.
[40] M. Kaminski, "Determination of transmission patterns in multichannel data," *Phil. Trans. R. Soc. B*, vol. 360, pp. 947–952, 2005.
[41] K. Sameshima and L. A. Baccala, "Using partial directed coherence to describe neuronal ensemble interactions," *J. Neurosci. Methods*, vol. 94, no. 1, pp. 93–103, Dec. 12, 1999.
[42] E. E. Fanselow *et al.*, "Thalamic bursting in rats during different awake behavioral states," *Proc. Nat. Acad. Sci.*, vol. 98, no. 26, pp. 15330–15335, 2001.
[43] M. Eichler, "On the evaluation of information flow in multivariate systems by the directed transfer function," *Biological Cybern.*, vol. 94, pp. 469–482, 2006.
[44] E. W. Lothman *et al.*, "Recurrent spontaneous hippocampal seizures in the rat as a chronic sequela to limbic status epilepticus," *Epilepsy. Res.*, vol. 6, no. 2, pp. 110–118, July 1990.
[45] J. C. Sanchez *et al.*, "Evolving into epilepsy: Multiscale electrophysiological analysis and imaging in an animal model," *Exp. Neurol.*, vol. 198, no. 1, pp. 31–47, Mar. 2006.
[46] E. H. Bertram and E. W. Lothman, "Morphometric effects of intermittent kindled seizures and limbic status epilepticus in the dentate gyrus of the rat," *Brain Res.*, vol. 603, no. 1, pp. 25–31, 1993.
[47] M. Quigg *et al.*, "Volumetric magnetic resonance imaging of bilateral hippocampal atrophy in mesial temporal lobe epilepsy," *Epilepsia.*, vol. 38, no. 5, pp. 588–594, 1997.
[48] M. Quigg *et al.*, "Temporal distribution of partial seizures: Comparison of an animal model with human partial epilepsy," *Ann. Neurol.*, pp. 748–755, 1998.
[49] S. Talathi, D. U. Hwang, M. L. Spano, J. Simonotto, M. D. Furman, S. M. Myers, J. T. Winters, W. L. Ditto, and P. R. Carney, "Non-parametric early seizure detection in an animal model of temporal lobe epilepsy," *J. Neural Eng.*, vol. 5, pp. 85–98.
[50] M. Morf, "Recursive multichannel maximum entropy spectral estimation," *IEEE Trans. Geosci. Electron.*, vol. GE-16, no. 2, pp. 85–94, Apr. 1978.
[51] E. Bertram *et al.*, "Functional anatomy of limbic epilepsy: A proposal for central synchronization of a diffusely hyperexcitable network," *Epilepsy. Res.*, vol. 32, pp. 194–205, 1998.
[52] D. Amaral and P. Lavenex, , P. Andersen, Ed., "Hippocampal neuroanatomy," in *The Hippocampus Book*. Oxford, U.K.: Oxford Univ. Press, 2007, pp. 37–114, et al.
[53] J. Zhong *et al.*, "Reversible, reproducible reduction of brain water apparent diffusion coefficient by cortical electroshocks," *Magn. Reson. Med.*, vol. 37, pp. 1–6, 1997.
[54] D. Ffytche and M. Catani, "Beyond localisation: From hodology to function," *Philos. Trans. R. Soc. Lond. B. Biol. Sci.*, no. 360, pp. 767–779, 2005, vol..
[55] H. Torrey, "Bloch equations with diffusion terms," *Phys. Rev.*, vol. 104, pp. 563–565, 1956.
[56] E. Stejskal, "Use of spin echoes in a pulsed magnetic-field gradient to study anisotropic, restricted diffusion and flow," *J. Chem. Phys.*, vol. 43, pp. 3597–3603, 1965.
[57] P. Basser, J. Mattiello, and D. LeBihan, "Estimation of the effective self-diffusion tensor from the NMR spin echo," *J. Magn. Reson. Ser. B*, vol. 103, pp. 247–354, 1994.
[58] P. Basser *et al.*, "In vivo fiber tractography using DT-MRI data," *Magn. Reson. Med.*, vol. 44, pp. 625–632, 2000.
[59] P. Basser and C. Pierpaoli, "Microstructural and physiological features of tissues elucidated by quantitative-diffusion-tensor MRI," *J. Magn. Reson. B*, vol. 111, pp. 209–219, 1996.
[60] T. Conturo *et al.*, "Tracking neuronal fiber pathways in the living human brain," *Proc. Nat. Acad. Sci. USA*, vol. 96, pp. 10422–10427, 1999.
[61] S. Mori *et al.*, "Three-dimensional tracking of axonal projections in the brain by magnetic resonance imaging," *Ann. Neurol.*, vol. 45, pp. 265–269, 1999.
[62] P. Basser, "Inferring microstructural features and the physiological state of tissues from diffusion-weighted images," *NMR Biomed.*, vol. 8, pp. 333–344, 1995.
[63] J. Zhong *et al.*, "Changes in water diffusion and relaxation properties of rat cerebrum during status epilepticus," *Magn. Reson. Med.*, vol. 30, no. 2, pp. 241–246, 1993.
[64] C. J. Wall, E. J. Kendall, and A. Obenaus, "Rapid alterations in diffusion-weighted images with anatomic correlates in a rodent model of status epilepticus," *AJNR Am. J. Neuroradiol.*, vol. 21, no. 10, pp. 1841–1852, 2000.
[65] Y. Nakasu *et al.*, "Diffusion-weighted MR in experimental sustained seizures elicited with kainic acid," *AJNR Am. J. Neuroradiol.*, vol. 16, no. 6, pp. 1185–1192, 1995.
[66] T. Engelhorn *et al.*, "Monitoring of acute generalized status epilepticus using multilocal diffusion MR imaging: Early prediction of regional neuronal damage," *AJNR Am. J. Neuroradiol.*, vol. 28, no. 2, pp. 321–327, Feb. 2007.
[67] J. W. Hugg, E. J. Butterworth, and R. I. Kuzniecky, "Diffusion mapping applied to mesial temporal lobe epilepsy: Preliminary observations," *Neurology*, vol. 53, no. 1, pp. 173–176, Jul. 13, 1999.
[68] B. A. Assaf *et al.*, "Diffusion tensor imaging of the hippocampal formation in temporal lobe epilepsy," *AJNR Am. J. Neuroradiol.*, vol. 24, no. 9, pp. 1857–1862, Oct. 2003.
[69] N. K. Focke *et al.*, "Voxel-based diffusion tensor imaging in patients with mesial temporal lobe epilepsy and hippocampal sclerosis," *Neuroimage*, vol. 40, no. 2, pp. 728–737, Apr. 1, 2008.
[70] D. W. Gross, L. Concha, and C. Beaulieu, "Extratemporal white matter abnormalities in mesial temporal lobe epilepsy demonstrated with diffusion tensor imaging," *Epilepsia*, vol. 47, no. 8, pp. 1360–1363, Aug. 2006.
[71] K. Arfanakis *et al.*, "Diffusion tensor MRI in temporal lobe epilepsy," *Magn. Reson. Imag.*, vol. 20, no. 7, pp. 511–519, Sep. 2002.
[72] S. Kim *et al.*, "Diffusion tensor MRI in rat models of invasive and well-demarcated brain tumors," *NMR Biomed.*, May 25, 2007.
[73] L. Concha, C. Beaulieu, and D. W. Gross, "Bilateral limbic diffusion abnormalities in unilateral temporal lobe epilepsy," *Ann. Neurol.*, vol. 57, no. 2, pp. 188–196, 2005.
[74] L. Concha *et al.*, "Bilateral white matter diffusion changes persist after epilepsy surgery," *Epilepsia*, vol. 48, no. 5, pp. 931–940, May 2007.
[75] M. Wiegell, H. Larsson, and V. Wedeen, "Fiber crossing in human brain depicted with diffusion tensor MR imaging," *Radiology*, vol. 217, pp. 897–903, 2000.
[76] E. von dem Hagen and R. Henkelman, "Orientational diffusion reflects fiber structure within a voxel," *Magn. Reson. Med.*, vol. 48, pp. 454–459, 2002.
[77] D. Tuch *et al.*, "Conductivity mapping of biological tissue using diffusion MRI," *Ann. NY Acad. Sci.*, vol. 888, pp. 314–316, 1999.
[78] D. Tuch *et al.*, "High angular resolution diffusion imaging reveals intravoxel white matter fiber heterogeneity," *Magn. Reson. Med.*, vol. 48, pp. 577–582, 2002.
[79] E. Ozarslan and T. H. Mareci, "Generalized diffusion tensor imaging and analytical relationships between diffusion tensor imaging and high angular resolution diffusion imaging," *Magn. Reson. Med.*, vol. 50, pp. 955–965, 2003.

[80] E. Ozarslan *et al.*, "Observation of anomalous diffusion in excised tissue by characterizing the diffusion-time dependence of the MR signal," *J. Magn. Reson.*, vol. 183, pp. 323–, 2006.
[81] B. Jian *et al.*, "A novel tensor distribution model for the diffusion-weighted MR signal," *Neuro. Image*, vol. 37, pp. 164–176, 2007.
[82] E. Ozarslan, B. C. Vemuri, and T. H. Mareci, "Generalized scalar measures for diffusion MRI using trace, variance, and entropy," *Magn. Reson. Med.*, vol. 53, pp. 866–876, 2005.
[83] T. Shepherd *et al.*, "Structural insights from high-resolution diffusion tensor imaging and tractography of the isolated rat hippocampus," *Neuro. Image*, vol. 32, pp. 1499–1509, 2006.
[84] F. Crick and E. Jones, "Backwardness of human neuroanatomy," *Nature*, vol. 361, pp. 109–110, 1993.
[85] J. Gotman, "Epileptic networks studied with EEG-fMRI," *Epilepsia*, vol. 49, pp. 42–51, 2008.

Alex J. Cadotte was born in Glens Falls, NY. He received the B.S. degree in chemical engineering from Virginia Tech, Blacksburg, in 1999, and the Ph.D. degree in biomedical engineering from the University of Florida, Gainesville, in 2007.

He is currently a Postdoctoral Fellow with the Neurology Division of the Department of Pediatrics and the Department of Biomedical Engineering at the University of Florida. His current research interests include structure function relationships in the vivo brain, neural networks, multivariate signal processing, neural engineering, tissue engineering, and epilepsy.

Thomas H. Mareci received the B.S. and M.S. degrees in physics from the University of Florida, in 1972 and 1979, respectively , and the Ph.D. in physical chemistry from the University of Oxford, Oxford, U.K., in 1982.

Currently he is a Professor in the Department of Biochemistry and Molecular Biology of the University of Florida. His research interests include the study of brain structure and fiber mapping using diffusion-based magnetic resonance imaging methods, the development of inductively-coupled implanted coils for monitoring deep tissues (e.g., spinal cord), and the study of changes in nervous tissue structure and function following injury.

Thomas B. DeMarse received the M.S. degree and the Ph.D. degree in learning and memory from Purdue University, in 1992 and 1997, respectively.

From 1997 to 1999 he worked as a Postdoctoral Researcher at Arizona State University and from 1999 to 2003 in the Biology Department at the California Institute of Technology and the Biomedical Engineering Department at Georgia Tech. He is currently an Assistant Professor in the Department of Biomedical Engineering at the University of Florida. His research interests include neural computation, neural interface technology, learning and memory in neural systems, and neural disorders such as epilepsy

Mansi B. Parekh received the B.S. degree in chemistry, in 2005, from University of Florida, Gainesville, where she is currently a graduate student in the Department of Neuroscience.

Her research interests include epileptogenesis, MRI, and brain connectivity.

Rajasimhan Rajagovindan received the B.E. degree in electronics and communication engineering from the University of Madras, Chennai, India, in 2004, and the M.S. degree in biomedical engineering, in 2008, from University of Florida, Gainesville, where he is currently pursuing the Ph.D. degree in biomedical engineering.

His research interests include biomedical signal processing, multivariate time series analysis, functional connectivity in the brain in behaving monkeys and humans, and the study of neural mechanisms of attentional control and memory.

William Ditto was born in Anchorage, AK. He received the B.S. degree in physics from the University of California, Los Angeles, in 1980, and the Ph.D. degree in physics from Clemson University, Clemson, SC, in 1988.

In 2002 he became the founding Chair of the Department of Biomedical Engineering at the University of Florida. In 2009 he became the Chair of the Biological Engineering Department at Arizona State University. His current work involves the development of therapies and devices for the control of epilepsy and the imaging of cardiac systems.

Sachin S. Talathi originally hails from Mumbai, India. He obtained his undergraduate education in engineering physics from Indian Institute of Technology Bombay, in 2001, and received the Ph.D. degree in physics from University of California–San Diego, in 2006.

He is currently a Research Assistant Professor with the Department of Biomedical Engineering at the University of Florida studying the dynamics of plastic changes brain networks following brain injury.

Dong-Uk Hwang received the Ph.D. degree in physics from Sogang University, Seoul, Korea.

He moved to the Neuroscience Laboratory at Chungbuk University (Korea) and worked on synchronization between neuronal oscillators and participated in EEG experiments to devise human–computer interfaces. From 2004 to 2005, he worked in the National Institute of Applied Optics, Florence, Italy, performing research on the dynamical properties in complex networks. From 2006 until now, he has been working as post-doc associate at University of Florida. He is currently working on developing methods to controlling neural activity preventing epileptic seizures.

Paul R. Carney completed basic neuroscience research and pediatric medical training at Case Western Reserve University, Cleveland, OH, and postdoctoral studies in pediatric neurology and neurophysiology at The University of Michigan Medical Center, Ann Arbor.

He is Wilder Chair Professor of Pediatrics, Neurology, Neuroscience, and Biomedical Engineering, at the University of Florida. His research has included several NIH sponsored interdisciplinary projects investigating the pathophysiology of epilepsy and sleep disorders, and the development and application of new technology for the diagnosis and treatment of epilepsy.